Jurnal Kejuruteraan 36(3) 2024: 1217–1226
https://doi.org/10.17576/jkukm-2024-36(3)-31

Physical and Hardness Performance at Different Surfaces for Titanium Alloy (Ti6Al4V) Printed Using Selective Laser Melting Process (SLM)

Farhana Mohd Foudzi[a,b*], Lai Yu Hung[a,b], Fathin Iliana Jamhari[a,b], Minhalina Ahmad Buhairi[a,b,c], Abu Bakar Sulong[a,b], Norhamidi Muhamad[a,b], Nabilah Afiqah Mohd Radzuan[a,b], Izhar Aziz[d] & Kim Seah Tan[e]

[a]*Advanced Manufacturing Research Group, Universiti Kebangsaan Malaysia, 43600 Bangi, Selangor, Malaysia*

[b]*Department of Mechanical and Manufacturing Engineering, Faculty of Engineering and Built Environment, Universiti Kebangsaan Malaysia, 43600 Bangi, Selangor, Malaysia*

[c]*Doctoral School on Materials Science and Technologies, Óbuda University, Nepszinhaz u. 8, 1081 Budapest, Hungary*

[d]*3D Gens Sdn Bhd, No 18, Jalan Kerawang U8/108, Bukit Jelutong, 40150 Shah Alam, Selangor, Malaysia*

[e]*Oryx Advanced Materials Sdn Bhd, Plot 69(d) & (e), Lintang Bayan Lepas 6, Bayan Lepas Industrial Zone, Phase 4, Bayan Lepas, 11900 Penang, Malaysia*

[*]*Corresponding author: farhana.foudzi@ukm.edu.my*

Received 8 January 2024, Received in revised form 5 April 2024
Accepted 5 May 2024, Available online 30 May 2024

ABSTRACT

Selective laser melting (SLM) 3D product is capable of producing varied surfaces such as top, core and bottom surface depending on the product dimensions and building orientation. Each surface may have differences in physical and mechanical properties such as surface roughness, microhardness, and microstructure. Therefore, this study examined the effects of SLM processing parameters as well as volumetric energy density (VED) on surface roughness, microhardness and microstructure on different 3D product surfaces. In this study, a sample of titanium alloy cube (Ti6Al4V) with different surfaces of up skin 1 (US1), up skin 2 (US2), core skin (CS) and down skin (DS) are printed on a 30° building orientation printed through the SLM process. There are nine sets of parameters printed based on the Taguchi experimental design method. All printed cube samples were heat treated to remove the residual stresses generated during the printing process. The effect of processing parameters on micro hardness as well as microstructure on each surface has been studied. This study found that SLM printed Ti6Al4V produced almost identical surface quality for different surfaces of the cubic samples. Surface roughness of US2 ranging between 15.38 µm and 26.22 µm, while DS is slightly rougher with surface roughness in the range of 16.05 µm and 27.64 µm. Microhardness in the nine processing sets however was found to have a bigger difference in values of 387 ± 10 HV (US2) and 362 ± 10 HV (DS). In general, US2 surfaces were found to have high microhardness compared to the DS surfaces due to the formation of long, straight needle-like martensitic microstructure.

Keywords: Selective Laser Melting, Processing parameter, Surface roughness, Microhardness

INTRODUCTION

Selective laser melting (SLM) is one of the most widely used additive manufacturing processes (AM) for metal materials, based on powder melting. It can be defined as the process by which 3D components can be produced by selectively scanning and fusing powder beds in a coating manner. SLM provides many advantages over conventional processes such as the ability to create complex geometry with internal cavities or features without die or specific tools, reducing lead time from design to test, reducing the need for installation, and the connectivity process resulting in less production costs (Nie et al. 2018; Syed et al. 2019). With the use of high energy laser beam to melt powders, this process also allows for high performance and high thermal properties metallic materials to be manufactured through rapid prototyping (Mohammed et al. 2019). High performing metals parts such as titanium alloy, Ti6Al4V have been commonly manufactured through SLM (Do & Li 2016; Louw & Pistorius 2019; Tarik Hasib et al. 2021). Ti6Al4V is a titanium alloy with superior strength, high corrosion resistance and good biocompatibility while being lightweight (Bartolomeu et al. 2022; Chunxiang et al. 2011; Maskery et al. 2015; Xu et al. 2015). This makes the metal, an apt choice for applications in marine, bio-implants and aerospace industries (Sarker et al. 2019; Wanying et al. 2017).

However, the main disadvantages of this process include the uniform quality of the specimens produced in terms of mechanical properties, production rates, dimensional accuracy that cause surface finish requirements and surface quality problems (Kumar & Ramamurty 2020). Surface quality is an important engineering aspect of the parts produced as it has a significant impact on the performance and durability of the parts. Many properties of parts such as wear, corrosion, fatigue depend on surface quality (Jamhari et al. 2023; Mohammed et al. 2019).

SLM involves heating and melting of powder with laser beam and rapid solidification of liquid material to form the desired component. There are several important physical phenomena for the process, such as the absorption of powder from laser irradiation, the phenomenon of roller that interfere with the formation of continuous melting, and the thermal fluctuations experienced by the material during the process which can lead to high residual stress, crack formation and component failure (Amirjan & Sakiani 2019; Andreacola et al. 2021; Jiang et al. 2020; Li et al. 2020; Rae 2019). In SLM, laser power (P), scanning speed (V), hatching distance (D), and layer thickness (T) are common process parameters that are customized to optimize the process (Buhairi et al. 2022). The volumetric energy density formula results from the relationship of these variables as shown in Equation (1).

$$Energy\ density\ \left(\frac{J}{mm^3}\right) = \frac{P\ (W)}{V\left(\frac{mm}{s}\right)\times T\ (mm)\times D(mm)} \quad (1)$$

Together with the absorption of powder into laser irradiation, these parameters affect the volumetric energy density available to heat and melting the powder. When heating and melting occur, heat and heat capacity should be considered. It depends on the material and is proportional to the mass to be melted. Insufficient energy, usually a combination of low laser power, high scanning speed, and large layer thickness, often results in balling due to lack of melting pool with previous layers (Mazlan et al. 2023). However, high lasers and low scanning speeds can result in extensive material evaporation and keyhole effects (Martin et al. 2019; Wen et al. 2018). In addition, poor hatching distances often result in porosity due to the adjacent melting line is not fully integrated (Derahman et al. 2018). Moreover, vaporization in SLM often results in condensation of the solvent in the laser window, interfering with laser energy transmission. Therefore, the combination of appropriate laser power, scanning speed, hatching distance, and coating thickness is crucial for SLM processing to successfully build full density parts. This study aims to study the effects of processing parameters as well as energy density on the surface roughness, microhardness and microstructure of titanium alloy printed using SLM.

METHODOLOGY

MATERIALS SELECTION

The raw material used in this study was Ti6Al4V grade 23 powder which has very low inter-space for SLM process. A preliminary characterisation of the Ti6Al4V powder used has been reported in a previous literature (Foudzi et al. 2022). The powder has a chemical composition containing 90% titanium, 6% aluminum, 4% vanadium, 0.25% iron and 0.2% oxygen. Particle size of the powder used ranges from 30μm to 70μm in spherical shape.

SAMPLE PREPARATION

This study employed the SLM 280HL printing machine to produce 1cm^3 Ti6Al4V cubic samples. Table 1 shows each processing parameter used to print the cubic samples with three levels showing three different values. Note that the layer height remains constant for all printing processes at a value of 0.03 mm. Nine sets of parameters were

developed from the default machine processing parameters with the use the Taguchi method. Past papers have reported a success in using this DOE method to reduce sample cost and generate a robust parameter set (Arifin et al. 2017; Omoniyi et al. 2021). Table 2 shows the different energy density values for each set of parameters. Energy density is calculated using Equation (1). The SLM process is performed in the following ranges: laser power (225 - 325 W), scan speed (800 - 1400 mm / s), hatching distance (0.10 - 0.14 mm), and layer height (0.03 mm).

TABLE 1. Factors (processing parameters) at different levels for the Taguchi method

Factor	Stage	
	0	1
Laser power (W)	225	275
Layer height (mm)	0.03	0.03
Hatching distance (mm)	0.10	0.12
Scanning speed (mm/s)	800	1100

TABLE 2. Processing parameters and energy density on all sets of parameters (P1 - P9)

Parameter sets	Laser power (W)	Layer height (mm)	Hatching distance (mm)	Scanning speed (mm/s)	Energy density
P1	225	0.03	0.10	800	93.75
P2	275	0.03	0.12	1100	69.44
P3	325	0.03	0.14	1400	55.27
P4	325	0.03	0.10	1100	98.50
P5	225	0.03	0.12	1400	44.64
P6	275	0.03	0.14	800	81.85
P7	275	0.03	0.10	1400	65.48
P8	325	0.03	0.12	800	112.85
P9	225	0.03	0.14	1100	48.70

The printing of cube specimens in this study also follows the building orientation shown in Figure 1. Before printing, the STL.file design was simulated using a software called Magics where appropriate building orientation was provided. The simulated build orientation gives the best build orientation value is 30.

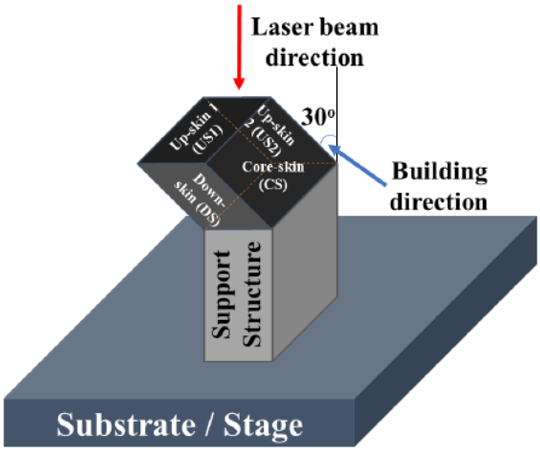

FIGURE 1. Schematic diagram for the cubic sample SLM printed

The printed cubic samples were heat treated with annealing process to relieve residual stress from SLM printing. The annealing process requires the material above the crystallization temperature for a specified period before cooling. In this study, the heat treatment temperature value used was 935oC with a heating rate of 7.35/minutes and the furnace cooling rate from 935oC to 70oC is 1.802/min.

SURFACE ROUGHNESS TEST

Surface roughness tests were performed using cube specimens printed through selective laser melting and the results of the study were recorded. The surface roughness test laboratory was launched in the Universiti Kebangsaan Malaysia laboratory room and the machine used was the Veeco Dektak 150 Machine. A total of 18 specimens were involved in this test and the results of each of the 3 readings were recorded on the surface of the specimen to obtain a more accurate average result. A total of 9 sets of parameter processing have been used to print specimens and study two surfaces of each set of parameter processing, namely up-skin 2 (US2) and down-skin (DS).

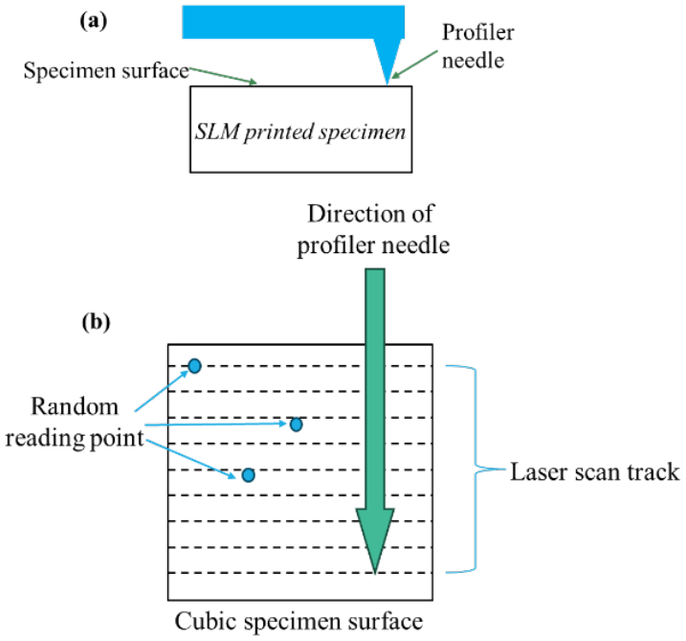

FIGURE 2. Schematic diagram for surface roughness measurements. (a) Profiler needle on specimen surface. (b) Surface roughness measurements.

MICROHARDNESS TEST

Microhardness tests were conducted on the cubic samples using the Micro-Vickers Zwick, ZHVμ machine according to the ASTM E384-11 standard in the Universiti Kebangsaan Malaysia laboratory room. A dwell time of 15 seconds with load of HV0.3 were applied during the microhardness test. Nine (9) random points were measured on each surface and averaged to obtain the most accurate microhardness results in this study.

MICROSTRUCTURE ANALYSIS

Microstructure analysis was performed on 9 sets of specimens. The surface of each specimen were prepared through grinding with SiC paper, polishing with diamond suspensions and etching using Keller's reagent with etching time of 10 seconds. The microstructure images were observed using an optical microscope, Mitutoyo. This microstructure analysis focused on the alpha, α and beta, β phases that form martensites that will determine the mechanical properties of the specimen.

RESULTS AND DISCUSSION

SURFACE ROUGHNESS TEST

Based on the results obtained from the surface roughness laboratory for up-skin 2 (US2), it is found that most

specimens have a surface roughness of less than 20 µm except P2, P7 and P8 specimens. Where the P8 specimen had the highest roughness of 26.22 µm while the lowest Ra value was the P9 specimen of 15.38 µm based on the the data obtained through laboratory testing. Meanwhile, it is found that down-skin (DS) have a surface roughness in the range of 16.05 µm and 27.64 µm in which specimen P9 has the smoothest and P8 has the roughest surface respectively. DS has a slightly higher than US2 due to the presence of support structure which was cut from the surface. Support structure is used for heat management during SLM printing. The effects of energy density on surface roughness obtained in this study can be observed in Figure 3.

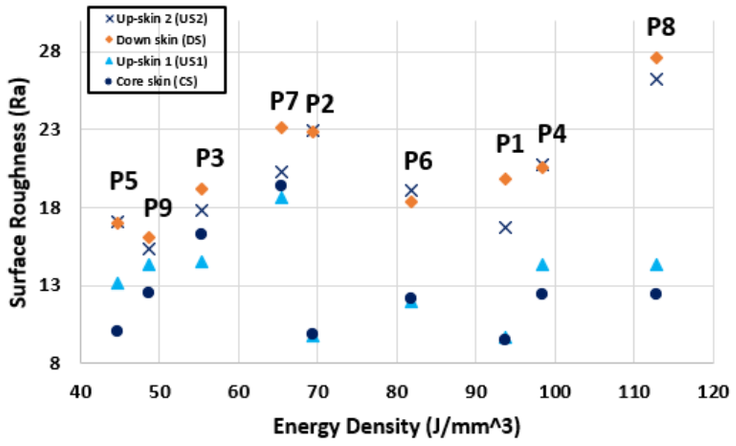

FIGURE 3. Graph surface roughness test for up-skin 1 (US1), up-skin 2 (US2), core skin (CS) and down skin (DS)

TABLE 3. Selected specimen processing parameter

Set	Laser power (W)	Layer height (mm)	Hatching distance (mm)	Scanning speed (mm/s)	Energy density (J/mm^3)
8	325	0.03	0.12	800	112.85
9	225	0.03	0.14	1100	48.70

Table 3 compares selected processing parameters where both specimens are a set of P8 and P9 specimen processing parameters that give the highest and lowest Ra values respectively. Compared to the processing parameters between the P8 and P9 specimens, the significant differences are the scanning speed and energy density parameters. Based on a recent study by Aufa et al. (2022), spattering in significant metal melting pools will occur when laser power is emitted at low scanning speeds. The effect of this spattering phenomenon has given the P8 specimen a rougher surface. In general, it can be concluded that with a laser power range of 225-275W and a scanning speed range of 1100mm/s can produce optimum surface roughness.

MICROHARDNESS TEST

Figure 4 shows the results obtained from the microhardness measurements of US2 and DS compared to their respective SLM printing energy density. Note that the results for upskin 1 (US 1) and core skin (CS) has been reported in a previous study (Foudzi et al. 2021). It is found that the P6 specimen had the highest hardness value of 404.1HV on average while the P1 specimen was the lowest of 370.0HV on average and the P5 specimen had a moderate hardness value among all specimens, 386.9HV. Meanwhile, microhardness measurements on DS specimens found that the P9 specimen had the highest hardness value of 378.0HV on average while the P3 specimen was the lowest of 327.0HV on average and the P5 specimen had a moderate hardness value among all specimens, 362.3HV.

A set of P1 and P6 specimen processing parameters that provide the lowest and highest HV values for the up-skin 2 (US2), while the P3 and P9 specimen processing parameters provide the lowest and highest HV values for the down skin (DS). Compared to the processing parameters between the P1 and P6 specimens, the significant differences are the hatching distance parameters and laser power. High hatching and laser power can produce the highest micro hardness specimens. Table 4 tabulates these four processing parameters for selected specimens.

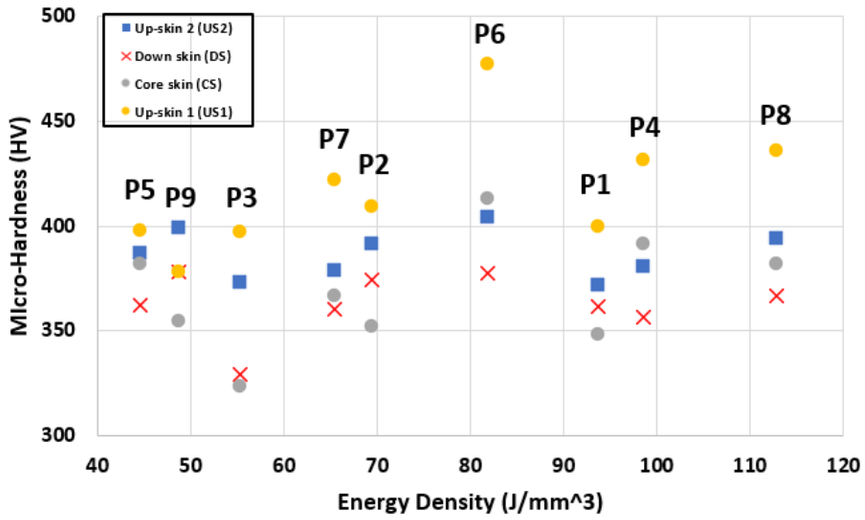

FIGURE 4. Graph microhardness test for up-skin 1 (US1), up-skin 2 (US2), core skin (CS) and down skin (DS

TABLE 4. Selected specimen processing parameter

No	Laser power (W)	Layer height (mm)	Hatching distance (mm)	Scanning speed (mm/s)	Energy density (J/mm3)
P1	225	0.03	0.10	800	93.75
P3	325	0.03	0.14	1400	55.27
P6	275	0.03	0.14	800	81.85
P9	225	0.03	0.14	1100	48.70

Furthermore, for the down skin study compared to the processing parameters between the P3 and P9 specimens, significant differences were laser power parameters and scanning speed. 325W laser power and 1400 mm/s scanning speed produce the lowest microhardness of the specimen. In general, it can be concluded that with a laser power range of 225-275W and a scanning speed range of 1100–1400mm/s can produce optimal microhardness.

MICROSTRUCTURE ANALYSIS

Based on the observations of the microstructure diagram in Figure 5 of specimens P2 (a,b), P7 (c,d), and P6 (e,f), the structure can be attributed to the obtained microhardness values. For the P6 specimen in which the highest microhardness value, it is found that the β phase is more apparent than that of other specimens. This specimen also has a good martensite between the β phase and α phase where the martensite is needle-like and straight (90). Whereas poor martensite distribution can be seen in specimens P2 (a,b) and P7 (c,d). In addition, it was found that specimens P3 (g,h), had pores which caused in a lower microhardness. In general, high micro hardness values can be obtained if the formation of a tapering, long, and 90 tang martensite is produced.

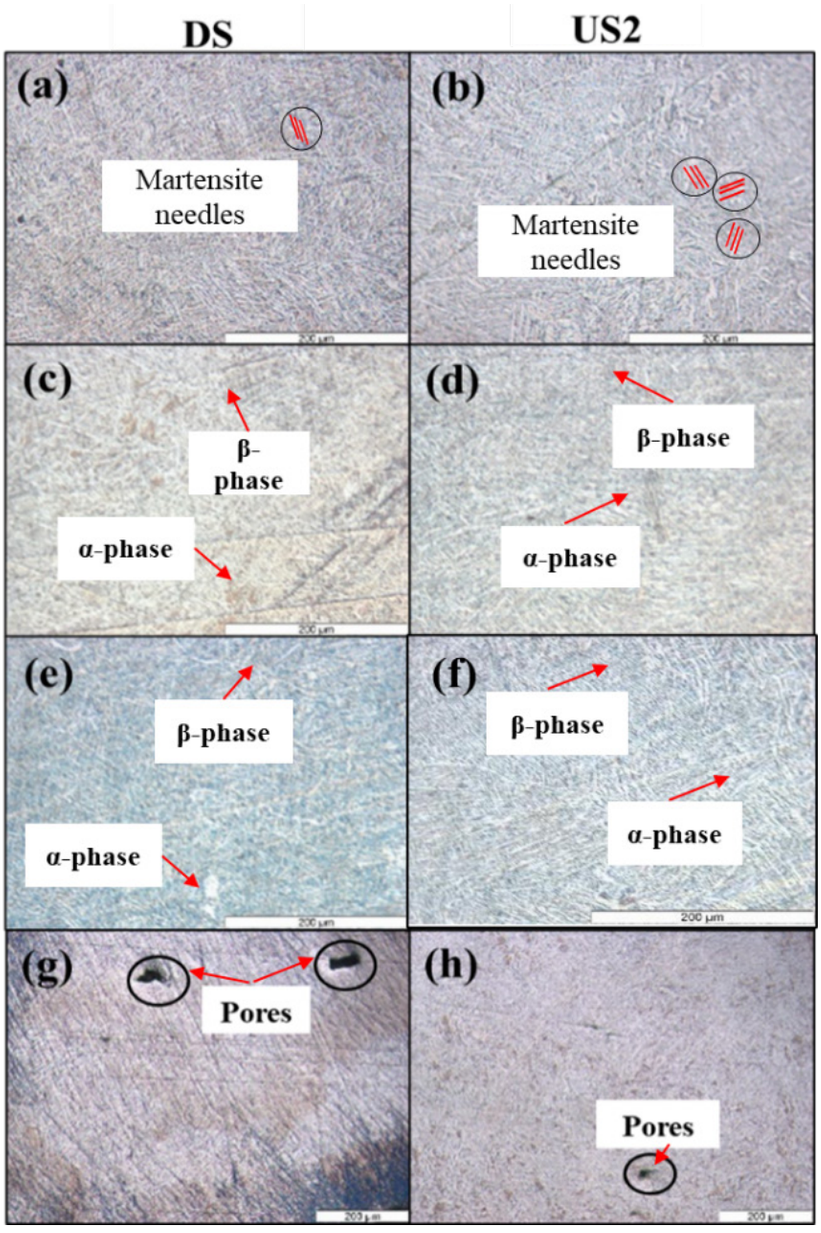

FIGURE 5. Microscope images for specimens P2 (a,b), P7 (c,d), P6 (e,f) and P3 (g,h)

ANALYSIS

SURFACE ROUGHNESS

Based on the previous study by Do & Li (2016) which investigated the relationship between energy density and mechanical properties. They reported that the density of energy is not a dominant parameter for the surface roughness of the specimen due to the fact that there is no pattern to be observed while the scanning speed is a dominant parameter due to the increased scanning speed, the surface roughness value of the specimen is increased no matter which surface. Similar results have been shown in the previous study Sadali et al. (2020) that the spattering phenomenon has occurred due to high scanning speed and has caused the specimen surface to be very rough compared to specimens produced at lower speeds. However, Table 5 compares P8 and P9 specimen processing parameters that give the highest and lowest Ra values. Compared to the processing parameters between the P8 and P9 specimens, the significant differences are the scanning speed parameters and energy density. Based on a recent study by (Sadali et al. 2020), spattering in significant metal melting pools will occur when laser power is emitted at low

scanning speeds. The effect of this spattering phenomenon has given the P8 specimen a rougher surface. In general, it can be concluded that lower laser power can produce more appropriate and lower surface roughness. Based on Table 5 this study has shown that laser power is the dominant parameter, and the scanning speed is not the dominant parameter because P2 and P9 have a scanning speed of 1100mm/s and laser power increases from 225 W (P9) up to 325 W (P8) have resulted in rougher surface roughness. These recent studies have been a supporter of this study as both reported a similar pattern showing increasing laser power would result in rougher surfaces. As such, this study has determined that the laser power influences the physical properties of the specimens in the selective laser melting process with the use of Titanium Ti6Al4V alloy metal material. In general, it can be concluded that with a laser power range of 225-275W and a scanning speed range of 1100mm/s can produce optimum surface roughness.

TABLE 5. Selected specimen processing parameter

No	Laser power (W)	Layer height (mm)	Hatching distance (mm)	Scanning speed (mm/s)	Energy density (J/mm3)
P2	275	0.03	0.12	1100	69.44
P8	325	0.03	0.12	800	112.85
P9	225	0.03	0.14	1100	48.70

MICROHARDNESS TEST

Popovich et al. (2016) discussed the mechanical properties of Titanium Ti6Al4V alloy metal products are highly dependent on the formation of martensites made from alpha and beta phases. From this discussion, it is possible to compare all the parameters by which the parameters have a significant effect on the formation of martensitic phases. Meanwhile, Ali et al. (2017) showed that the highest density was achieved in samples built with 200W laser power and 100μs exposure time, produces components with minimum defects and density of 99.99%. The study also conducted a microhardness test on the existing specimen and reported similar findings with this study. In that increasing the energy density would increase the value of the hardness of metal parts. Moreover, it was concluded that with a laser power range of 225 – 275W and a scanning speed range of 1100 – 1400mm/s can produce optimal microhardness, and this proves that laser power is the dominant processing parameter for the mechanical properties of microhardness.

MICROSTRUCTURE ANALYSIS

Popovich et al. (2015) had also performed microstructure analysis using variations in heat treatment. It was reported that beta and alpha martensite formation are key to the formation of high physical and mechanical properties of samples. In this regard, comparisons were made between microstructure analysis and microscopy images in this study. The well-known martensite has been found to be sharp, long, and thin, with straight tapered (90 °) showing excellent properties. Energy density is not a dominant processing parameter because the energy density is indirectly proportional to microhardness. The pores that arise in the specimen will also cause mechanical properties to be disrupted and become worse. Based on the report by Saunders (2018), some of the defects that would commonly occur with unoptimised processing window include lack of fusion, balling and keyhole formation. Moreover, it was found that the combination of laser power parameters and scanning speed should be determined appropriately for optimal mechanical properties of the specimen. If lower laser power is used with high scanning speed, then the melting pool will be smaller. This means that it may experience less turbulence and produce less spattering as it hardens faster. The implication is that lower laser energy may not penetrate deep enough to completely melt the powder coating and solid metal surface below. This leaves the powder unmelted under the liquid pool, leading to excess porosity and melting risk as reported in past study (Foudzi et al. 2021). This is true in specimens P1 and P3 where this specimen is found in pores.

CONCLUSION

This study has successfully investigated the effect of varied processing parameters on physical and mechanical properties of different surfaces for Ti6Al4V printed through SLM. Based on the results obtained in this study for up-skin 2 (US2), the surface roughness for the varied parameter sets were in the range of 15.38 μm and 26.22 μm obtained from parameter sets P9 and P8 respectively. Meanwhile, it is found that down-skin (DS) have a surface roughness in the range of 16.05 μm and 27.64 μm in which specimen P9 has the smoothest and P8 has the roughest surface respectively. The slight difference in surface quality of both surfaces is attributed to the varied scan speed and energy density. The effect of spattering phenomenon has given the P8 specimen a rougher surface. In general, it can be concluded that with a laser power range of 225-275W and a scanning speed range of 1100mm/s can produce optimum surface roughness.

In addition, based on the results obtained from the microhardness test for US2, it is found that P6 had the highest hardness of 404.1HV while the P1 was the lowest with 371.98HV and the P5 had a moderate hardness value among all parameter sets, 386.87HV. For DS, it is found that P9 had the highest hardness value of 378.0HV while P4 was the lowest of 356.8HV and P5 had a moderate hardness value among all specimens, 362.3HV. The difference in hardness of both surfaces was attributed to the varied energy density due to laser power, scan speed and hatching distance. This study concluded that with a laser power range of 225-275W and a scanning speed range of 1100-1400mm/s can produce optimal microhardness. Hardness of the SLM-printed Ti6Al4V specimens was also discussed in relation to their microstructure observations. It is discussed that high microhardness can be obtained through the formation of long and needle-like martensite structure for α and β phases of Ti6Al4V alloy.

This study found that laser power and scanning speed greatly influenced the physical and mechanical properties of titanium alloy specimens printed via SLM. Through careful investigation into surface quality and microhardness, it is found that these two processing parameters contributed more than the other processing parameters on the performance of SLM printed parts. With the aim of producing a better microstructure with martensite crystal structure that meets the specific criteria for suitable application, considerations of the laser power and scanning speed is an important step.

ACKNOWLEDGEMENT

The authors would like to acknowledge Ministry of Higher Education (MOHE) for funding under the Fundamental Research Grant Scheme (FRGS) (FRGS/1/2019/TK03/UKM/02/5) and Center for Research and Instrumentation (CRIM) Universiti Kebangsaan Malaysia (UKM) under the Geran Universiti Penyelidikan (GUP) (GUP-2021-015) for this project. Authors would also like to acknowledge 3D Gens Sdn. Bhd. and Oryx Advanced Materials Sdn. Bhd. for providing the required facilities and knowledge transfer support to complete this study.

DECLARATION OF COMPETING INTEREST

None

REFERENCES

A.K. Syed, B. Ahmad, Guo, H., Machry, T., Eatock, D., Meyer, J. & Fitzpatrick, M.E. et al. 2019. An experimental study of residual stress and direction-dependence of fatigue crack growth behaviour in as-built and stress-relieved selective-laser-melted Ti6Al4V. *Materials Science and Engineering A* 755: 246–257.

Amir Arifin, Gunawan, Irsyadi Yani, Muhammad Yanis & Raka Pradifta. 2017. Optimization of stir casting method of aluminum matrix composite (AMC) for the hardness properties by using taguchi method. *Jurnal Kejuruteraan* 29(1): 35–39.

Andreacola, F.R., Capasso, I., Pilotti, L. & Brando, G. 2021. Influence of 3d-printing parameters on the mechanical properties of 17-4ph stainless steel produced through selective laser melting. *Frattura ed Integrita Strutturale* 15(58): 282–295.

A.N. Aufa, Mohamad Zaki Hassan, Zarini Ismail, Norhaslinda Harun, James Ren & Mohd Faizal Sadali. 2022. Surface enhancement of Ti–6Al–4V fabricated by selective laser melting on bone-like apatite formation. *Journal of Materials Research and Technology* 19: 4018–4030.

Bartolomeu, F., Gasik, M., Silva, F.S. & Miranda, G. 2022. Mechanical properties of Ti6Al4V fabricated by laser powder bed fusion: A review focused on the processing and microstructural parameters influence on the final properties. *Metals* 12(6).

Chunxiang Cui, Baomin Hu, Lichen Zhao & Shuangjin Liu. 2011. Titanium alloy production technology, market prospects and industry development. *Materials and Design* 32(3): 1684–1691.

F.I. Jamhari, F.M. Foudzi, M.A. Buhairi, N. Muhamad, I.F. Mohamed, A.B. Sulong & N.A.M. Radzuan. 2023. Impact of hot isostatic pressing on surface quality, porosity and performance of Ti6Al4V manufactured by laser powder bed fusion: A brief review. *Jurnal Tribologi* 36: 1–15.

Foudzi, F. M., Buhairi, M. A., Jamhari, F. I., Sulong, A. B., Harun, W. S. W. & Al-Furjan, M. S. H. 2021. Effect of Energy Density on Properties of Additive Manufactured Ti6Al4V via SLM. *Powder Met 21*, hlm. 434–449.

Foudzi, F. M., Jamhari, F. I. & Buhairi, M. A. 2022. Characterisation and Comparison of Titanium Alloy (Ti6Al4V) Powders Used in Selective Laser Melting (SLM). *Sains Malaysiana* 51(6): 1885–1894.

Haider Ali, Hassan Ghadbeigi & Kamran Mumtaz. 2018. Effect of scanning strategies on residual stress and mechanical properties of selective laser melted Ti6Al4V. *Materials Science and Engineering A* 712: 175–187.

Junfeng Li, Zhengying Wei, Lixiang Yang, Bokang Zhou, Yunxiao Wu, Sheng-Gui Chen & Zhenzhong Sun. 2020. Finite element analysis of thermal behavior and experimental investigation of Ti6Al4V in selective laser melting. *Optik* 207: 163760.

Khao Do & Peifeng Li. 2016. The effect of laser energy input on the microstructure, physical and mechanical properties of Ti-6Al-4V alloys by selective laser melting. *Virtual and Physical Prototyping* 11(1): 41–47. DOI:10.1080/17452759.2016.1142215

Kumar, P. & Ramamurty, U. 2020. High cycle fatigue in selective laser melted Ti-6Al-4V. *Acta Materialia* 194: 305–320.

Liu Wanying, Lin Yuanhua, Chen Yuhai, Shi Taihe & Ambrish Singh. 2017. Effect of different heat treatments on microstructure and mechanical properties of Ti6Al4V titanium alloy. *Rare Metal Materials and Engineering* 46(3): 634–639.

Louw, D.F. & Pistorius, P.G.H. 2019. The effect of scan speed and hatch distance on prior-beta grain size in laser powder bed fused Ti-6Al-4V. *International Journal of Advanced Manufacturing Technology* 103(5–8): 2277–2286.

Martin, A.A., Calta, N.P., Khairallah, S.A., Wang, J., Depond, P.J., Fong, A.Y., Thampy, V. et al. 2019. Dynamics of pore formation during laser powder bed fusion additive manufacturing. *Nature Communications* 10(1): 1–10.

M.A. Buhairi, F.M Foudzi, F.I. Jamhari, A.B. Sulong, N.A. Mohd Radzuan, N. Muhamad, I.F. Mohamed et al. 2022. Review on volumetric energy density: Influence on morphology and mechanical properties of Ti6Al4V manufactured via laser powder bed fusion. *Progress in Additive Manufacturing* 8(11).

Maskery, I., Aremu, A.O., Simonelli, M., Tuck, C., Wildman, R.D., Ashcroft, I.A. & Hague, R.J.M. 2015. Mechanical properties of Ti-6Al-4V selectively laser melted parts with body-centred-cubic lattices of varying cell size. *Experimental Mechanics* 55(7): 1261–1272.

M.F. Sadali, M.Z. Hassan, N.H. Ahmad, M.A. Suhot & R. Mohammad. 2020. Laser power implication to the hardness of Ti-6Al-4V powder by using SLM additive manufacturing technology. *Proceedings of Mechanical Engineering Research Day 2020*, 45-46.

Mohsin Talib Mohammed, Anton Sotov & Smelov V.G. 2019. SLM-built titanium materials: Great potential of developing microstructure and properties for biomedical applications: A review. *Material Research Express* 6(12): 10–13.

Mostafa Amirjan & Hassan Sakiani. 2019. Effect of scanning strategy and speed on the microstructure and mechanical properties of selective laser melted IN718 nickel-based superalloy. *International Journal of Advanced Manufacturing Technology* 103(5–8): 1769–1780.

M.R. Mazlan, N.H. Jamadon, A. Rajabi, A.B. Sulong, I.F. Mohamed, F. Yusof & N.A. Jamal. 2023. Necking mechanism under various sintering process parameters: A review. *Journal of Materials Research and Technology* 23: 2189–2201.

M. Tarik Hasib, Ostergaard, H.E., Xiaopeng Li & Kruzic, J.J. 2021. Fatigue crack growth behavior of laser powder bed fusion additive manufactured Ti-6Al-4V: Roles of post heat treatment and build orientation. *International Journal of Fatigue* 142: 105955.

N.A. Derahman, M. Sayuti, A. Karim, N. Amirah & M. Amran. 2018. Effects of process parameters on surface quality of parts produced by selective laser melting – ANFIS modelling. *Proceedings of Mechanical Engineering Research Day* 115–116.

Omoniyi, P.O., Mahamood, R.M., Arthur, N., Pityana, S., Akinlabi, S.A., Okamoto, Y., Maina, M.R. et al. 2021. Investigation and optimization of heat treatment process on tensile behaviour of Ti6Al4V alloy. *Materials Science & Engineering Technology* 52(10): 1057–1063.

Peng Wen, Jauer, L., Voshage, M., Yanzhe Chen, Poprawe, R. & Schleifenbaum, J.H. 2018. Densification behavior of pure Zn metal parts produced by selective laser melting for manufacturing biodegradable implants. *Journal of Materials Processing Technology* 258(2010): 128–137.

Rae, W. 2019. Thermo-metallo-mechanical modelling of heat treatment induced residual stress in Ti–6Al–4V alloy. *Materials Science and Technology (United Kingdom)* 35(7): 747–766.

Runbo Jiang, Amir Mostafaei, Ziheng Wu, Ann Choi, Pinwen Guan, Chmielus, M. & Rollett, A.D. 2020. Effect of heat treatment on microstructural evolution and hardness homogeneity in laser powder bed fusion of alloy 718. *Additive Manufacturing* 35: 101282.

Sarker, A., Tran, N., Rifai, A., Brandt, M., Tran, P.A., Leary, M., Fox, K. et al. 2019. Rational design of additively manufactured Ti6Al4V implants to control staphylococcus aureus biofilm formation. *Materialia* 5: 100250.

Saunders, M. 2018. How process parameters drive successful metal AM part production. *Metal AM* 4(2).

Wei Xu, Brandt, M., Shoujin Sun, Elambasseril, J., Qianchu Liu, Latham, K., Xia, K. et al. 2015. Additive manufacturing of strong and ductile Ti-6Al-4V by selective laser melting via in situ martensite decomposition. *Acta Materialia* 85: 74–84.

Xiaojia Nie, Hu Zhang, Haihong Zhu, Zhiheng Hu, Linda Ke & Xiaoyan Zeng. 2018. Analysis of processing parameters and characteristics of selective laser melted high strength Al-Cu-Mg alloys: From single tracks to cubic samples. *Journal of Materials Processing Technology* 256(2010): 69–77.